

Measurement of the Lepton Forward-Backward Asymmetry in $B \rightarrow X_s \ell^+ \ell^-$ Decays with a Sum of Exclusive Modes

Y. Sato,^{60,36} A. Ishikawa,⁶⁰ H. Yamamoto,⁶⁰ A. Abdesselam,⁵⁵ I. Adachi,¹² K. Adamczyk,⁴¹ H. Aihara,⁶¹
 D. M. Asner,⁴⁶ V. Aulchenko,⁴ T. Aushev,³⁴ R. Ayad,⁵⁵ A. M. Bakich,⁵⁴ A. Bala,⁴⁷ V. Bhardwaj,³⁷ B. Bhuyan,¹⁴
 A. Bondar,⁴ G. Bonvicini,⁶⁷ A. Bozek,⁴¹ M. Bračko,^{30,20} T. E. Browder,¹¹ D. Červenkov,⁵ V. Chekelian,³¹
 A. Chen,³⁸ B. G. Cheon,¹⁰ I.-S. Cho,⁶⁹ K. Cho,²⁴ V. Chobanova,³¹ Y. Choi,⁵³ D. Cinabro,⁶⁷ J. Dalseno,^{31,57}
 M. Danilov,³³ Z. Doležal,⁵ Z. Drásal,⁵ A. Drutskoy,³³ D. Dutta,¹⁴ K. Dutta,¹⁴ S. Eidelman,⁴ H. Farhat,⁶⁷
 J. E. Fast,⁴⁶ T. Ferber,⁸ V. Gaur,⁵⁶ A. Garmash,⁴ R. Gillard,⁶⁷ Y. M. Goh,¹⁰ B. Golob,^{28,20} J. Haba,¹² T. Hara,¹²
 K. Hayasaka,³⁶ H. Hayashii,³⁷ X. H. He,⁴⁸ Y. Hoshi,⁵⁹ W.-S. Hou,⁴⁰ H. J. Hyun,²⁶ T. Iijima,^{36,35} R. Itoh,¹²
 Y. Iwasaki,¹² T. Iwashita,²³ I. Jaegle,¹¹ T. Julius,³² J. H. Kang,⁶⁹ E. Kato,⁶⁰ Y. Kato,³⁵ H. Kawai,⁶ T. Kawasaki,⁴³
 H. Kichimi,¹² D. Y. Kim,⁵² H. J. Kim,²⁶ J. B. Kim,²⁵ J. H. Kim,²⁴ M. J. Kim,²⁶ Y. J. Kim,²⁴ K. Kinoshita,⁷
 J. Klucar,²⁰ B. R. Ko,²⁵ P. Kodyš,⁵ S. Korpar,^{30,20} P. Križan,^{28,20} P. Krokovny,⁴ T. Kuhr,²² T. Kumita,⁶³
 A. Kuzmin,⁴ Y.-J. Kwon,⁶⁹ S.-H. Lee,²⁵ Y. Li,⁶⁶ J. Libby,¹⁵ C. Liu,⁵¹ Y. Liu,⁷ Z. Q. Liu,¹⁶ D. Liventsev,¹²
 P. Lukin,⁴ H. Miyata,⁴³ R. Mizuk,^{33,34} G. B. Mohanty,⁵⁶ A. Moll,^{31,57} R. Mussa,¹⁹ M. Nakao,¹² Z. Natkaniec,⁴¹
 M. Nayak,¹⁵ E. Nedelkovska,³¹ N. K. Nisar,⁵⁶ S. Nishida,¹² O. Nitoh,⁶⁴ S. Ogawa,⁵⁸ P. Pakhlov,³³ H. Park,²⁶
 H. K. Park,²⁶ T. K. Pedlar,²⁹ T. Peng,⁵¹ R. Pestotnik,²⁰ M. Petrič,²⁰ L. E. Piilonen,⁶⁶ E. Ribežl,²⁰ M. Ritter,³¹
 M. Röhrken,²² A. Rostomyan,⁸ H. Sahoo,¹¹ T. Saito,⁶⁰ Y. Sakai,¹² S. Sandilya,⁵⁶ D. Santel,⁷ L. Santelj,²⁰
 T. Sanuki,⁶⁰ V. Savinov,⁴⁹ O. Schneider,²⁷ G. Schnell,^{1,13} C. Schwanda,¹⁷ A. J. Schwartz,⁷ R. Seidl,⁵⁰ D. Semmler,⁹
 K. Senyo,⁶⁸ M. E. Sevior,³² M. Shapkin,¹⁸ C. P. Shen,² T.-A. Shibata,⁶² J.-G. Shiu,⁴⁰ B. Shwartz,⁴ A. Sibidanov,⁵⁴
 F. Simon,^{31,57} Y.-S. Sohn,⁶⁹ A. Sokolov,¹⁸ E. Solovieva,³⁴ S. Stanič,⁴⁴ M. Starič,²⁰ T. Sumiyoshi,⁶³ U. Tamponi,^{19,65}
 G. Tatishvili,⁴⁶ Y. Teramoto,⁴⁵ K. Trabelsi,¹² M. Uchida,⁶² S. Uehara,¹² T. Uglov,³⁴ Y. Unno,¹⁰ S. Uno,¹²
 P. Urquijo,³ Y. Ushiroda,¹² Y. Usov,⁴ S. E. Vahsen,¹¹ C. Van Hulse,¹ P. Vanhoefer,³¹ G. Varner,¹¹ K. E. Varvell,⁵⁴
 V. Vorobyev,⁴ C. H. Wang,³⁹ M.-Z. Wang,⁴⁰ P. Wang,¹⁶ X. L. Wang,⁶⁶ Y. Watanabe,²¹ E. Won,²⁵ J. Yamaoka,⁴⁶
 Y. Yamashita,⁴² S. Yashchenko,⁸ Y. Yook,⁶⁹ Z. P. Zhang,⁵¹ V. Zhilich,⁴ V. Zhulanov,⁴ and A. Zupanc²⁰

(The Belle Collaboration)

¹University of the Basque Country UPV/EHU, 48080 Bilbao

²Beihang University, Beijing 100191

³University of Bonn, 53115 Bonn

⁴Budker Institute of Nuclear Physics SB RAS and Novosibirsk State University, Novosibirsk 630090

⁵Faculty of Mathematics and Physics, Charles University, 121 16 Prague

⁶Chiba University, Chiba 263-8522

⁷University of Cincinnati, Cincinnati, Ohio 45221

⁸Deutsches Elektronen-Synchrotron, 22607 Hamburg

⁹Justus-Liebig-Universität Gießen, 35392 Gießen

¹⁰Hanyang University, Seoul 133-791

¹¹University of Hawaii, Honolulu, Hawaii 96822

¹²High Energy Accelerator Research Organization (KEK), Tsukuba 305-0801

¹³IKERBASQUE, Basque Foundation for Science, 48011 Bilbao

¹⁴Indian Institute of Technology Guwahati, Assam 781039

¹⁵Indian Institute of Technology Madras, Chennai 600036

¹⁶Institute of High Energy Physics, Chinese Academy of Sciences, Beijing 100049

¹⁷Institute of High Energy Physics, Vienna 1050

¹⁸Institute for High Energy Physics, Protvino 142281

¹⁹INFN - Sezione di Torino, 10125 Torino

²⁰J. Stefan Institute, 1000 Ljubljana

²¹Kanagawa University, Yokohama 221-8686

²²Institut für Experimentelle Kernphysik, Karlsruher Institut für Technologie, 76131 Karlsruhe

²³Kavli Institute for the Physics and Mathematics of the Universe (WPI), University of Tokyo, Kashiwa 277-8583

²⁴Korea Institute of Science and Technology Information, Daejeon 305-806

²⁵Korea University, Seoul 136-713

²⁶Kyungpook National University, Daegu 702-701

²⁷École Polytechnique Fédérale de Lausanne (EPFL), Lausanne 1015

²⁸Faculty of Mathematics and Physics, University of Ljubljana, 1000 Ljubljana

²⁹Luther College, Decorah, Iowa 52101

³⁰University of Maribor, 2000 Maribor

³¹Max-Planck-Institut für Physik, 80805 München

³²School of Physics, University of Melbourne, Victoria 3010

- ³³ *Moscow Physical Engineering Institute, Moscow 115409*
- ³⁴ *Moscow Institute of Physics and Technology, Moscow Region 141700*
- ³⁵ *Graduate School of Science, Nagoya University, Nagoya 464-8602*
- ³⁶ *Kobayashi-Maskawa Institute, Nagoya University, Nagoya 464-8602*
- ³⁷ *Nara Women's University, Nara 630-8506*
- ³⁸ *National Central University, Chung-li 32054*
- ³⁹ *National United University, Miao Li 36003*
- ⁴⁰ *Department of Physics, National Taiwan University, Taipei 10617*
- ⁴¹ *H. Niewodniczanski Institute of Nuclear Physics, Krakow 31-342*
- ⁴² *Nippon Dental University, Niigata 951-8580*
- ⁴³ *Niigata University, Niigata 950-2181*
- ⁴⁴ *University of Nova Gorica, 5000 Nova Gorica*
- ⁴⁵ *Osaka City University, Osaka 558-8585*
- ⁴⁶ *Pacific Northwest National Laboratory, Richland, Washington 99352*
- ⁴⁷ *Panjab University, Chandigarh 160014*
- ⁴⁸ *Peking University, Beijing 100871*
- ⁴⁹ *University of Pittsburgh, Pittsburgh, Pennsylvania 15260*
- ⁵⁰ *RIKEN BNL Research Center, Upton, New York 11973*
- ⁵¹ *University of Science and Technology of China, Hefei 230026*
- ⁵² *Soongsil University, Seoul 156-743*
- ⁵³ *Sungkyunkwan University, Suwon 440-746*
- ⁵⁴ *School of Physics, University of Sydney, NSW 2006*
- ⁵⁵ *Department of Physics, Faculty of Science, University of Tabuk, Tabuk 71451*
- ⁵⁶ *Tata Institute of Fundamental Research, Mumbai 400005*
- ⁵⁷ *Excellence Cluster Universe, Technische Universität München, 85748 Garching*
- ⁵⁸ *Toho University, Funabashi 274-8510*
- ⁵⁹ *Tohoku Gakuin University, Tagajo 985-8537*
- ⁶⁰ *Tohoku University, Sendai 980-8578*
- ⁶¹ *Department of Physics, University of Tokyo, Tokyo 113-0033*
- ⁶² *Tokyo Institute of Technology, Tokyo 152-8550*
- ⁶³ *Tokyo Metropolitan University, Tokyo 192-0397*
- ⁶⁴ *Tokyo University of Agriculture and Technology, Tokyo 184-8588*
- ⁶⁵ *University of Torino, 10124 Torino*
- ⁶⁶ *CNP, Virginia Polytechnic Institute and State University, Blacksburg, Virginia 24061*
- ⁶⁷ *Wayne State University, Detroit, Michigan 48202*
- ⁶⁸ *Yamagata University, Yamagata 990-8560*
- ⁶⁹ *Yonsei University, Seoul 120-749*
- (Dated: May 7, 2019)

We report the first measurement of the lepton forward-backward asymmetry \mathcal{A}_{FB} as a function of the squared four-momentum of the dilepton system, q^2 , for the electroweak penguin process $B \rightarrow X_s \ell^+ \ell^-$ with a sum of exclusive final states, where ℓ is an electron or a muon and X_s is a hadronic recoil system with an s quark. The results are based on a data sample containing 772×10^6 $B\bar{B}$ pairs recorded at the $\Upsilon(4S)$ resonance with the Belle detector at the KEKB e^+e^- collider. \mathcal{A}_{FB} for the inclusive $B \rightarrow X_s \ell^+ \ell^-$ is extrapolated from the sum of 10 exclusive X_s states whose invariant mass is less than $2 \text{ GeV}/c^2$. For $q^2 > 10.2 \text{ GeV}^2/c^2$, $\mathcal{A}_{\text{FB}} < 0$ is excluded at the 2.3σ level, where σ is the standard deviation. For $q^2 < 4.3 \text{ GeV}^2/c^2$, the result is within 1.8σ of the Standard Model theoretical expectation.

PACS numbers: 11.30.Er, 11.30.Hv, 12.15.Ji, 13.20.He

I. INTRODUCTION

In the Standard Model (SM), quark-level flavor-changing neutral current $b \rightarrow s \ell^+ \ell^-$ decays [1] are allowed at higher order via the electroweak loop (penguin) and W^+W^- box diagrams. The corresponding decay amplitude can be expressed via the Operator Product Expansion [2] in terms of the effective Wilson coefficients for the electromagnetic penguin, C_7^{eff} , and the vector and axial-vector electroweak contributions, C_9^{eff} and C_{10}^{eff} , respectively [3]. If physics beyond the SM contributes

to $b \rightarrow s \ell^+ \ell^-$ decays, then the effective Wilson coefficients are expected to differ from the SM expectations. Therefore the decay rate and angular distributions of $b \rightarrow s \ell^+ \ell^-$ decays constitute good probes to search for new physics [4].

Inclusive measurements of the $b \rightarrow s \ell^+ \ell^-$ process are preferable to exclusive measurements because of lower theoretical uncertainties, although they are experimentally more challenging. The branching fraction for inclusive $B \rightarrow X_s \ell^+ \ell^-$, where B is either \bar{B}^0 or B^- , ℓ is either an electron or a muon, and X_s is a hadronic re-

coil system with an s quark, has been measured by Belle [5] and BABAR [6]. Both results are consistent with the SM prediction. The lepton forward-backward asymmetry, defined as

$$\mathcal{A}_{\text{FB}}(q_{\text{min}}^2, q_{\text{max}}^2) = \frac{\int_{q_{\text{min}}^2}^{q_{\text{max}}^2} dq^2 \int_{-1}^1 d\cos\theta \operatorname{sgn}(\cos\theta) \frac{d^2\Gamma}{dq^2 d\cos\theta}}{\int_{q_{\text{min}}^2}^{q_{\text{max}}^2} dq^2 \int_{-1}^1 d\cos\theta \frac{d^2\Gamma}{dq^2 d\cos\theta}} \quad (1)$$

is considered to have different and greater sensitivity to physics beyond the SM than the branching fraction [7, 8]. Here, q^2 is the squared four-momentum of the dilepton system and θ is the angle between the $\ell^+(\ell^-)$ and the B meson momentum in the $\ell^+\ell^-$ center-of-mass frame in \bar{B}^0 or B^- (B^0 or B^+) decays. Although \mathcal{A}_{FB} in exclusive $B \rightarrow K^{(*)}\ell^+\ell^-$ has been measured by Belle [9], BABAR [10], CDF [11], LHCb [12] and CMS [13], \mathcal{A}_{FB} in inclusive $B \rightarrow X_s\ell^+\ell^-$ is yet to be measured. At lowest order, the numerator in Eq. 1 for inclusive $B \rightarrow X_s\ell^+\ell^-$ can be written [14] as a function of q^2

$$\int_{-1}^1 \operatorname{sgn}(\cos\theta) \frac{d^2\Gamma}{dq^2 d\cos\theta} d\cos\theta = -3\Gamma_0 m_b^3 c^8 (1-s)^2 s C_{10} \operatorname{Re} \left(C_9 + \frac{2}{s} C_7 \right), \quad (2)$$

where m_b is the b -quark mass, $s = q^2/(m_b^2 c^2)$, and $\Gamma_0 = \frac{G_F^2}{48\hbar^6 c^6 \pi^3} \frac{\alpha_{\text{em}}}{16\pi^2} |V_{tb} V_{ts}^*|^2$. Here, G_F is the Fermi coupling constant, V_{tb} and V_{ts} are Cabibbo-Kobayashi-Maskawa matrix elements [15], and α_{em} is the fine-structure constant.

We report the first measurement of the lepton forward-backward asymmetry for inclusive $B \rightarrow X_s\ell^+\ell^-$, which is extrapolated from the sum of 10 exclusive X_s states with an invariant mass $M_{X_s} < 2.0 \text{ GeV}/c^2$, corresponding to 50% of the inclusive rate. We also report this asymmetry for the subsamples of $B \rightarrow K^{(*)}\ell^+\ell^-$ with the X_s invariant mass $M_{X_s} < 1.1 \text{ GeV}/c^2$ and $B \rightarrow X_s\ell^+\ell^-$ with $M_{X_s} > 1.1 \text{ GeV}/c^2$, where this asymmetry for $B \rightarrow K\ell^+\ell^-$ is expected to be zero in the SM. We assume that \mathcal{A}_{FB} is independent of lepton flavor. When the final state X_s is not a $K^{(*)}$, we also assume \mathcal{A}_{FB} depends neither on X_s nor on the X_s mass. The results are based on the full $\Upsilon(4S)$ data sample containing $772 \times 10^6 \bar{B}B$ pairs recorded with the Belle detector [16] at the KEKB e^+e^- collider [17].

II. DETECTOR

The Belle detector is a general-purpose magnetic spectrometer which consists of a silicon vertex detector (SVD), a 50-layer central drift chamber (CDC), an array of aerogel threshold Cherenkov counters (ACC), time-of-flight scintillation counters (TOF), and an electromagnetic calorimeter (ECL) comprised of CsI(Tl) crystals. The devices are located inside a superconducting solenoid

coil that provides a 1.5 T magnetic field. An iron flux-return located outside the coil is instrumented to detect K_L^0 mesons and to identify muons (KLM). The detector is described in detail elsewhere [16].

III. SIGNAL MODEL

We study the acceptance for $B \rightarrow X_s\ell^+\ell^-$ via Monte Carlo (MC) simulation. For this simulation, we use a sum of exclusive $B \rightarrow K^{(*)}\ell^+\ell^-$ events and non-resonant $B \rightarrow X_s\ell^+\ell^-$ events with $M_{X_s} > 1.1 \text{ GeV}/c^2$. The former are generated according to Refs. [4, 18], while the latter are generated using a model based on Refs. [4, 19] and the Fermi motion model of Ref. [20]. The two MC samples are mixed assuming the measured branching fractions [21].

IV. EVENT SELECTION

Charged tracks are reconstructed with the SVD and CDC, and the tracks other than $K_S^0 \rightarrow \pi^+\pi^-$ daughters are required to originate from the interaction region. Electrons are identified by a combination of the specific ionization (dE/dx) in the CDC, the ratio of the cluster energy in the ECL to the track momentum measured with the SVD and CDC, the response of the ACC, the shower shape in the ECL, and position matching between the shower and the track. Muons are identified by the track penetration depth and hit scatter in the KLM. Electrons and muons are required to have momenta greater than 0.4 GeV/ c and 0.8 GeV/ c , respectively. To recover bremsstrahlung photons from leptons, we add the four-momentum of each photon detected within 0.05 rad of the original track direction. Charged kaons are identified by combining information from the dE/dx in the CDC, the flight time measured with the TOF, and the response of the ACC [22]. We select electron, muon, and kaon candidate tracks in turn, while the remaining tracks are assumed to be charged pions.

K_S^0 candidates are formed by combining two oppositely charged tracks, assuming both are pions with requirements on their invariant mass, flight length, and consistency between the K_S^0 momentum direction and vertex position. Neutral pion candidates are formed from pairs of photons that have an invariant mass within 10 MeV/ c^2 of the nominal π^0 mass, where photons are measured as an energy cluster in the ECL with no associated charged tracks. Neutral pions and their photon daughters are required to have an energy greater than 400 MeV and 50 MeV, respectively. A mass-constrained fit is then performed to obtain the π^0 momentum.

We reconstruct X_s from 18 hadronic final states (see Table I), that consist of one K^\pm or K_S^0 and up to four pions, of which at most one can be neutral. To reject a large part of the combinatorial background, we require $M_{X_s} < 2 \text{ GeV}/c^2$, which preserves 91% of signal.

TABLE I. The 18 hadronic final states used to reconstruct X_s . The 8 final states enclosed in parentheses are not used for the measurement of \mathcal{A}_{FB} .

B^0 decays		B^- decays	
$K^- \pi^+$	(K_S^0)	K^-	
$K^- \pi^+ \pi^0$	$(K_S^0 \pi^0)$	$K^- \pi^0$	$K_S^0 \pi^-$
$K^- \pi^+ \pi^- \pi^+$	$(K_S^0 \pi^- \pi^+)$	$K^- \pi^+ \pi^-$	$K_S^0 \pi^- \pi^0$
$K^- \pi^+ \pi^- \pi^+$	$(K_S^0 \pi^- \pi^+ \pi^0)$	$K^- \pi^+ \pi^- \pi^0$	$K_S^0 \pi^- \pi^+ \pi^-$
$(K^- \pi^+ \pi^- \pi^+ \pi^0)$	$(K_S^0 \pi^- \pi^+ \pi^- \pi^+)$	$(K^- \pi^+ \pi^- \pi^+ \pi^-)$	$(K_S^0 \pi^- \pi^+ \pi^- \pi^0)$

We combine the X_s with two oppositely charged leptons to form a B meson candidate. To identify the signal, we use two kinematic variables defined in the $\Upsilon(4S)$ rest frame: the beam-energy constrained mass $M_{\text{bc}} = \sqrt{E_{\text{beam}}^{*2} - |\vec{p}_B|^2}$, and the energy difference $\Delta E = E_B - E_{\text{beam}}^*$, where E_{beam}^* is the beam energy and (\vec{p}_B, E_B) is the reconstructed momentum and energy of the B candidate. We require $M_{\text{bc}} > 5.22 \text{ GeV}/c^2$ and $-100 \text{ MeV} < \Delta E < 50 \text{ MeV}$ ($-50 \text{ MeV} < \Delta E < 50 \text{ MeV}$) for the electron (muon) channel.

To reject large contamination from charmonium backgrounds $B \rightarrow J/\psi(\psi(2S))X_s$ followed by $J/\psi(\psi(2S)) \rightarrow \ell^+ \ell^-$, we reject events having dilepton invariant mass in the following veto regions: -400 to $150 \text{ MeV}/c^2$ (-250 to $100 \text{ MeV}/c^2$) around the J/ψ mass and -250 to $100 \text{ MeV}/c^2$ (-150 to $100 \text{ MeV}/c^2$) around the $\psi(2S)$ mass for the electron (muon) channel. In the electron channel, there is non-negligible peaking background from events in which the bremsstrahlung photon recovery fails and instead the radiated photon together with another random photon forms a misreconstructed π^0 as X_s 's daughter. To veto such events, the π^0 's photon daughter with the highest energy is added in the calculation of the dilepton invariant mass, and events with invariant mass from $150 \text{ MeV}/c^2$ below to $50 \text{ MeV}/c^2$ above the nominal J/ψ mass are rejected for the modes involving π^0 . We also require the dilepton mass to be greater than $0.2 \text{ GeV}/c^2$ to remove the photon conversion and π^0 Dalitz decays.

V. BACKGROUND SUPPRESSION

The main background comes from random combinations of two semileptonic B or D decays, which have both large missing energy due to neutrinos, and displaced origin of leptons from B or D mesons. The displacement between the two leptons is measured by the distance $\Delta z_{\ell^+ \ell^-}$ between the points of closest approach to the beam axis along the beam direction. We also use the confidence level of the B vertex (\mathcal{C}_{vtx}), constructed from all charged daughter particles except for K_S^0 daughters. We set requirements on $\Delta z_{\ell^+ \ell^-}$ and \mathcal{C}_{vtx} to preserve about 79% of the signal while rejecting 66% of the background. Other background originates from $e^+ e^- \rightarrow q \bar{q}$ ($q = u, d, s, c$) continuum events, which can be efficiently suppressed using event shape variables.

To suppress the continuum background and further

reduce the semileptonic background, we employ a neural network based on the software package ‘‘NeuroBayes’’ [23]. The inputs to the network are (i) a likelihood ratio based on ΔE , (ii) the cosine of the angle between the B candidate and the beam axis in the $\Upsilon(4S)$ rest frame, (iii) $\Delta z_{\ell^+ \ell^-}$, (iv) \mathcal{C}_{vtx} , (v) the total visible energy, (vi) the missing mass [24], and (vii) 17 event shape variables based on modified Fox-Wolfram moments [25]. For the different types of backgrounds (semileptonic and continuum), the neural network is trained separately and requirements on two output values are chosen to maximize the statistical significance. This optimization is performed separately for electron and muon channels and for the regions $M_{X_s} < 1.1 \text{ GeV}/c^2$ and $M_{X_s} > 1.1 \text{ GeV}/c^2$, and the obtained selection preserves 51% (63%) of the signal while rejecting 98% (96%) of the background for electron (muon) channels. According to the MC simulation, 83% of the remaining background consists of semileptonic events.

The probability of multiple B candidates in a signal event is 8% with the average number of B candidates per signal event being 1.1. When multiple B candidates are found in an event, we select the most signal-like B candidate based on the neural network output. For the measurement of \mathcal{A}_{FB} , information on the flavor of the B candidate is necessary. For \bar{B}^0 mesons, only the self-tagging modes with a K^- are kept, after selecting one B candidate per event. We also remove candidates with X_s reconstructed from one kaon plus four pions because expected signal yields are less than one event. Therefore, we use 10 final states as listed in Table I for the X_s to measure \mathcal{A}_{FB} .

VI. MAXIMUM LIKELIHOOD FIT

To examine the q^2 dependence of \mathcal{A}_{FB} , we divide the data into 4 bins of measured q^2 : $[0.2, 4.3]$, $[4.3, 7.3(8.1)]$, $[10.5(10.2), 11.8(12.5)]$, $[14.3, 25.0] \text{ GeV}^2/c^2$ for the electron (muon) channel, where the gap regions correspond to the veto regions for charmonium background events. The bins are numbered in the order of increasing q^2 ; the lowest q^2 for bin number 1, and the highest for bin number 4. In order to extract \mathcal{A}_{FB} , an extended unbinned maximum likelihood fit to four M_{bc} distributions (positive/negative $\cos \theta$ for electron/muon channel) is simultaneously performed for each q^2 bin. We also measure \mathcal{A}_{FB} in the low- q^2 region, $1 < q^2 < 6 \text{ GeV}^2/c^2$, where it is theoretically clean.

The raw asymmetry $\mathcal{A}_{\text{FB}}^{\text{raw}} = \frac{N(\cos \theta > 0) - N(\cos \theta < 0)}{N(\cos \theta > 0) + N(\cos \theta < 0)}$, where N is the observed signal yields, differs from \mathcal{A}_{FB} due to the dependence of the signal reconstruction efficiency on q^2 and $\cos \theta$. Figure 1 show the reconstruction efficiencies on a plane of q^2 and $\cos \theta$. This pronounced dependence arises from events with low q^2 and high $\cos \theta$ having lepton momenta below the event selection requirements. We define α as a scaling factor that relates $\mathcal{A}_{\text{FB}}^{\text{raw}}$ to \mathcal{A}_{FB} . We assume that \mathcal{A}_{FB} does not depend on the

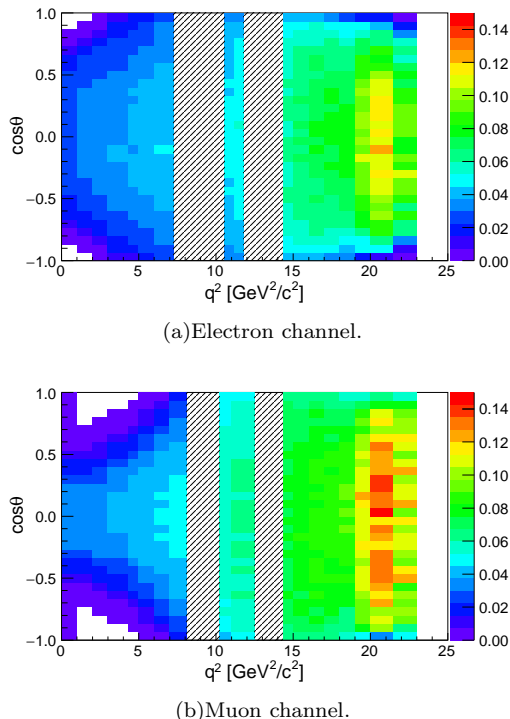


FIG. 1. Reconstruction efficiency on a plane of q^2 and $\cos\theta$ for (a) the electron and (b) the muon channels. The J/ψ and $\psi(2S)$ veto regions are shown as hatched regions.

lepton flavor. However, \mathcal{A}_{FB} in the second and third q^2 bins do differ between electron and muon channels due to the distinct charmonium-veto regions. We identify \mathcal{A}_{FB} as the fit parameter for the q^2 regions of the muon channel and then introduce the scaling factor β between the values in the electron and muon channels. With these factors, the fit parameter \mathcal{A}_{FB} is

$$\begin{aligned} \mathcal{A}_{\text{FB}} &\equiv \mathcal{A}_{\text{FB}}^{\mu\mu} \\ &= \beta \cdot \mathcal{A}_{\text{FB}}^{ee}, \text{ where} \\ \mathcal{A}_{\text{FB}}^{\ell\ell} &= \alpha^{\ell\ell} \cdot \mathcal{A}_{\text{FB}}^{\text{raw},\ell\ell} \quad (\ell = e, \mu). \end{aligned} \quad (3)$$

To derive $\alpha^{\ell\ell}$ ($\ell = e, \mu$), we generate several sets of signal MC samples with various Wilson coefficients (C_7, C_9, C_{10}), and calculate $\mathcal{A}_{\text{FB}}^{\ell\ell}$ for each set. We evaluate $\mathcal{A}_{\text{FB}}^{\text{raw},\ell\ell}$ using the reconstruction efficiency as a function of q^2 and $\cos\theta$. We derive $\alpha^{\ell\ell}$ by fitting the relation between $\mathcal{A}_{\text{FB}}^{\ell\ell}$ and $\mathcal{A}_{\text{FB}}^{\text{raw},\ell\ell}$ to a straight line. In the first q^2 bin, the quite distinct values of α between electron and muon channels reflect the different lepton momentum selection criteria. To derive β , we fit the relation between $\mathcal{A}_{\text{FB}}^{ee}$ and $\mathcal{A}_{\text{FB}}^{\mu\mu}$ in the same way. The values of α and β are summarized in Table II.

The likelihood function consists of four components: signal, self cross-feed, combinatorial background, and peaking background. The signal is modeled with a Gaussian function with parameters obtained from the $B \rightarrow J/\psi X_s$ data. The self cross-feed is described by

a MC histogram, where the yield ratio to the signal is fixed according to the MC expectation. The combinatorial background is modeled by an ARGUS function [26], where the endpoint is fixed to the nominal beam energy in the $\Upsilon(4S)$ rest frame, $E_{\text{beam}}^* = 5.289$ GeV. We have three peaking background sources. First is charmonium peaking background, $B \rightarrow J/\psi(\psi(2S))X_s$ decays with The yields and shape of these charmonium peaking backgrounds is modeled by histogram shape of charmonium MC samples. The yields of charmonium peaking background are estimated to be 0.9 ± 0.2 and 2.1 ± 0.2 events in the electron and muon channels, respectively. We treat contributions from charmonium resonances higher than $\psi(2S)$ as signal. Second is $B \rightarrow D^{(*)}n\pi$ ($n > 0$) decay with misidentification of two charged pions as two leptons. The yields and shape of this peaking background is determined directly from the data by performing the analysis without the lepton identification requirements. Taking the $\pi \rightarrow \ell$ misidentification rates into account, We estimate this peaking background to be 0.07 ± 0.01 and 5.0 ± 0.2 events in the electron and muon channels, respectively. Third is $B \rightarrow J/\psi(\psi(2S))X_s$ with swapped misidentification between a lepton and a pion. The yields and shape of this peaking background is determined directly from the data by performing the analysis selecting dilepton invariant mass around J/ψ and $\psi(2S)$. Taking the $\pi \rightarrow \ell$ misidentification rates and particle identification efficiencies into account, we estimate this peaking background to be 0.06 ± 0.02 and 4.3 ± 0.2 events in the electron and muon channels, respectively.

VII. SYSTEMATIC UNCERTAINTIES

To estimate systematic uncertainties, we repeat the \mathcal{A}_{FB} fit with varied input parameters and the resulting change in \mathcal{A}_{FB} is taken as the systematic uncertainty for the varied parameter. Systematic uncertainties for \mathcal{A}_{FB} are summarized in Table III. In the 1st q^2 bin, the dominant systematic uncertainty arises from the translation of $\mathcal{A}_{\text{FB}}^{\text{raw}}$ to \mathcal{A}_{FB} with α and β . Even if a MC sample with a different set of Wilson coefficients produces the same values of \mathcal{A}_{FB} , the $\mathcal{A}_{\text{FB}}^{\text{raw}}$ values and hence the α coefficient may differ. It gives rise to an uncertainty of the offset in the linear fit. To estimate this uncertainty, the relation between $\mathcal{A}_{\text{FB}}^{\text{raw}}$ and \mathcal{A}_{FB} are projected onto the axis perpendicular to the fitted linear line and fitted by a Gaussian function. To estimate systematic uncertainties from the peaking background, the yield of each such background is varied by its uncertainty. For the charmonium peaking background, the yield is varied by $\pm 100\%$, conservatively, because it is determined from MC events. A possible peaking background from $B \rightarrow Kn\pi\ell\nu$ ($n > 0$), where one pion is misidentified as a lepton and the missing neutrino is compensated by a pion of the other B decay, is examined. The number of events in the whole q^2 region is estimated from MC to be 0.2 ± 0.6 (1.1 ± 0.7) for electron (muon) channel,

TABLE II. Fit results for the five q^2 bins. For \mathcal{A}_{FB} , the first uncertainty is statistical and the second uncertainty is systematic. \mathcal{A}_{FB} values predicted by the SM [4, 7] are also shown with systematic uncertainties. For the signal yields, only statistical uncertainties are shown. The uncertainties of α and β are due to the statistical uncertainties of the MC.

	1st q^2 bin	2nd q^2 bin	3rd q^2 bin	4th q^2 bin	
q^2 range [GeV^2/c^2]	[0.2, 4.3]	$[4.3, 7.3]_{X_s e^+ e^-}$ $[4.3, 8.1]_{X_s \mu^+ \mu^-}$	$[10.5, 11.8]_{X_s e^+ e^-}$ $[10.2, 12.5]_{X_s \mu^+ \mu^-}$	[14.3, 25.0]	[1.0, 6.0]
\mathcal{A}_{FB}	$0.34 \pm 0.24 \pm 0.03$	$0.04 \pm 0.31 \pm 0.05$	$0.28 \pm 0.21 \pm 0.02$	$0.28 \pm 0.15 \pm 0.02$	$0.30 \pm 0.24 \pm 0.04$
\mathcal{A}_{FB} (theory)	-0.11 ± 0.03	0.13 ± 0.03	0.32 ± 0.04	0.40 ± 0.04	-0.07 ± 0.04
N_{sig}^{ee}	45.6 ± 10.9	30.0 ± 9.2	25.0 ± 7.0	39.2 ± 9.6	50.3 ± 11.4
$N_{\text{sig}}^{\mu\mu}$	43.4 ± 9.2	23.9 ± 10.4	30.7 ± 9.9	62.8 ± 10.4	35.3 ± 9.2
α^{ee}	1.289 ± 0.004	1.139 ± 0.003	1.063 ± 0.003	1.121 ± 0.003	1.255 ± 0.003
$\alpha^{\mu\mu}$	2.082 ± 0.010	1.375 ± 0.003	1.033 ± 0.003	1.082 ± 0.003	1.863 ± 0.006
β	1.000	1.019 ± 0.003	1.003 ± 0.000	1.000	1.000

and the resulting systematic error is $\mathcal{O}(0.001)$. In the 2nd q^2 bin, the systematic uncertainty from charmonium peaking background is dominant. To estimate the systematic uncertainties from signal modeling, the related parameters are varied. The fraction of $B \rightarrow K^{(*)}\ell^+\ell^-$ and non-resonant $B \rightarrow X_s\ell^+\ell^-$ are varied within experimental uncertainties. $B \rightarrow K^{(*)}\ell^+\ell^-$ MC samples are generated with different form factors [27, 28]. The Fermi motion parameter is varied in accordance with measurements of hadronic moments in semileptonic B decays [29] and the photon spectrum in inclusive $B \rightarrow X_s\gamma$ decays [30]. The b -quark pole mass is varied by ± 0.15 GeV/c^2 around 4.80 GeV/c^2 . The threshold point of non-resonant $B \rightarrow X_s\ell^+\ell^-$ events is varied by ± 100 MeV/c^2 around $M_{X_s} = 1.1$ GeV/c^2 . In the region $M_{X_s} < 1.1$ GeV/c^2 , there is possible contamination from the non-resonant S -wave component of the $K\pi$ system. Nevertheless, we find negligible systematic uncertainty from this effect by adding 5% contributions of S -wave components to the dominant K^* in this M_{X_s} region [31]. We check the hadronization process in the non-resonant $B \rightarrow X_s\ell^+\ell^-$ events by comparing the $B \rightarrow J/\psi X_s$ events in data and MC simulations. To estimate the systematic uncertainties related to X_s spin components, we generate non-resonant $B \rightarrow X_s\ell^+\ell^-$ MC samples with spin 0 and 1 using the form factor for $B \rightarrow K^{(*)}\ell^+\ell^-$. In these MC samples, X_s always decays to the two-body $K\pi$ final states to enhance the effect of the X_s spin. We replace the nominal non-resonant $B \rightarrow X_s\ell^+\ell^-$ MC samples with these MC samples, and estimate the systematic uncertainty from the difference between MC samples with spin 0 and 1. The signal shape parameters are fixed using the $J/\psi X_s$ data. The mean and width of the signal Gaussian function are varied within their uncertainties. The histogram shape of the self cross-feed background is estimated from signal MC events. The entries in the bins are varied according to a Gaussian distribution whose standard deviation is the statistical uncertainty of the MC sample. The total systematic uncertainty is estimated by summing the above uncertainties in quadrature.

VIII. FORWARD-BACKWARD ASYMMETRY

Figure 2, 3, 4, 5, and 6 show the M_{bc} distributions for $B \rightarrow X_s e^+ e^-$ and $B \rightarrow X_s \mu^+ \mu^-$ candidates with positive and negative $\cos\theta$ in each q^2 bin. The total signal yields for $B \rightarrow X_s e^+ e^-$ and $B \rightarrow X_s \mu^+ \mu^-$ are 140 ± 19 (stat) and 161 ± 20 (stat), respectively. The fit results obtained in each q^2 bins are summarized in Table II. Figure 7 shows the \mathcal{A}_{FB} distribution as a function of q^2 . The \mathcal{A}_{FB} results are found to be consistent with the SM prediction in the 2nd to 4th q^2 bins, while it deviates from the SM in the 1st q^2 bin by 1.8σ ; here, the systematic uncertainty is taken into account. The results in the 3rd and 4th bin also excludes $\mathcal{A}_{\text{FB}} < 0$ at the 2.3σ level.

To distinguish the contributions from $B \rightarrow K\ell^+\ell^-$, $B \rightarrow K^*\ell^+\ell^-$, and non- $K^{(*)}\ell^+\ell^-$ candidates, we divide the samples into distinct M_{X_s} ranges and extract \mathcal{A}_{FB} by the same fitting method. Table IV shows the \mathcal{A}_{FB} values in each subsample. \mathcal{A}_{FB} in $B \rightarrow K\ell^+\ell^-$ is consistent with null, as expected in the SM, while \mathcal{A}_{FB} in $B \rightarrow K^*\ell^+\ell^-$ is consistent with previous measurements [9–13].

IX. CONCLUSION

In conclusion, we report the first measurement of the lepton forward-backward asymmetry for the electroweak penguin process $B \rightarrow X_s\ell^+\ell^-$ using a data sample containing 772×10^6 $B\bar{B}$ pairs collected with the Belle detector. \mathcal{A}_{FB} for the inclusive $B \rightarrow X_s\ell^+\ell^-$ is extrapolated from the sum of 10 exclusive X_s states, assuming \mathcal{A}_{FB} depends neither on the lepton flavor nor on the X_s mass. For $q^2 > 10.2$ GeV^2/c^2 , $\mathcal{A}_{\text{FB}} < 0$ is excluded at the 2.3σ level. For $q^2 < 4.3$ GeV^2/c^2 , the result is within 1.8σ of the SM expectation. The results can be used to constrain various extensions of the SM.

X. ACKNOWLEDGMENT

We thank T. Morozumi and T. Goto for their invaluable suggestions. We thank the KEKB group for the

TABLE III. Summary of systematic uncertainties in the five q^2 bins.

Sources of uncertainties	1st q^2 bin	2nd q^2 bin	3rd q^2 bin	4th q^2 bin	$1 < q^2 < 6 \text{ GeV}^2/c^2$
Translation from $\mathcal{A}_{\text{FB}}^{\text{raw}}$ to \mathcal{A}_{FB}	0.019	0.013	0.007	0.003	0.020
Peaking background	0.004	0.050	0.007	0.002	0.021
Signal modeling	0.018	0.003	0.021	0.017	0.019
Signal shape and self cross-feed	0.002	0.002	0.002	0.002	0.002
Total	0.027	0.052	0.023	0.017	0.035

TABLE IV. Fit results for subsamples of (i) $B \rightarrow K\ell^+\ell^-$, (ii) $B \rightarrow K^-\pi^+\ell^+\ell^-$, $K^-\pi^0\ell^+\ell^-$, or $K_S^0\pi^-\ell^+\ell^-$ with $M_{X_s} < 1.1 \text{ GeV}/c^2$, and (iii) $B \rightarrow X_s\ell^+\ell^-$ with $M_{X_s} > 1.1 \text{ GeV}/c^2$ for the five q^2 bins. The uncertainty includes only statistical uncertainty. Unfortunately, \mathcal{A}_{FB} for $B \rightarrow K\ell^+\ell^-$ can not be obtained in 3rd q^2 bin, due to too low statistics.

State	1st q^2 bin	2nd q^2 bin	3rd q^2 bin	4th q^2 bin	$1 < q^2 < 6 \text{ GeV}^2/c^2$
K	-0.05 ± 0.24	-0.11 ± 0.29	n.a.	0.12 ± 0.18	0.00 ± 0.13
K^* with $M_{X_s} < 1.1 \text{ GeV}/c^2$	0.62 ± 0.42	0.20 ± 0.33	0.01 ± 0.34	0.21 ± 0.22	0.55 ± 0.43
X_s with $M_{X_s} > 1.1 \text{ GeV}/c^2$	0.25 ± 0.45	0.97 ± 0.60	0.92 ± 0.32	0.65 ± 0.54	0.74 ± 0.54

excellent operation of the accelerator; the KEK cryogenics group for the efficient operation of the solenoid; and the KEK computer group, the National Institute of Informatics, and the PNNL/EMSL computing group for valuable computing and SINET4 network support. We acknowledge support from the Ministry of Education, Culture, Sports, Science, and Technology (MEXT) of Japan, the Japan Society for the Promotion of Science (JSPS), and the Tau-Lepton Physics Research Center of Nagoya University; the Australian Research Council; Austrian Science Fund under Grant No. P 22742-N16 and P 26794-N20; the National Natural Science Foundation of China under Contracts No. 10575109, No. 10775142, No. 10875115, No. 11175187, No. 11475187 and No. 11575017; the Chinese Academy of Science Center for Excellence in Particle Physics; the Ministry of Education, Youth and Sports of the Czech Republic under Contract No. LG14034; the Carl Zeiss Foundation, the Deutsche Forschungsgemeinschaft, the Excellence Cluster Universe, and the VolkswagenStiftung; the Department of Science and Technology of India; the Istituto Nazionale di Fisica Nucleare of Italy; the WCU program of the Ministry of Education, National

Research Foundation (NRF) of Korea Grants No. 2011-0029457, No. 2012-0008143, No. 2012R1A1A2008330, No. 2013R1A1A3007772, No. 2014R1A2A2A01005286, No. 2014R1A2A2A01002734, No. 2015R1A2A2A01003280, No. 2015H1A2A1033649; the Basic Research Lab program under NRF Grant No. KRF-2011-0020333, Center for Korean J-PARC Users, No. NRF-2013K1A3A7A06056592; the Brain Korea 21-Plus program and Radiation Science Research Institute; the Polish Ministry of Science and Higher Education and the National Science Center; the Ministry of Education and Science of the Russian Federation and the Russian Foundation for Basic Research; the Slovenian Research Agency; Ikerbasque, Basque Foundation for Science and the Euskal Herriko Unibertsitatea (UPV/EHU) under program UFI 11/55 (Spain); the Swiss National Science Foundation; the Ministry of Education and the Ministry of Science and Technology of Taiwan; and the U.S. Department of Energy and the National Science Foundation. This work is supported by a Grant-in-Aid from MEXT for Science Research in a Priority Area (“New Development of Flavor Physics”) and from JSPS for Creative Scientific Research (“Evolution of Tau-lepton Physics”).

-
- [1] Charge-conjugate decays are implied throughout this paper, unless otherwise stated.
- [2] K. G. Wilson, *Phys. Rev.* **179**, 1499 (1969).
- [3] G. Buchalla, A.J. Buras, and M.E. Lautenbacher, *Rev. Mod. Phys.* **68**, 1125 (1996).
- [4] A. Ali, E. Lunghi, C. Greub, and G. Hiller, *Phys. Rev.* **D66**, 034002 (2002).
- [5] M. Iwasaki *et al.* (Belle Collaboration), *Phys. Rev.* **D72**, 092005 (2005).
- [6] B. Aubert *et al.* (BABAR Collaboration), *Phys. Rev. Lett.* **93**, 081802 (2004).
- [7] S. Fukae, C.S. Kim, T. Morozumi, and T. Yoshikawa, *Phys. Rev.* **D59**, 074013 (1999).
- [8] T. Huber, T. Hurth, and E. Lunghi, *Nucl. Phys.* **B802**, 40 (2008).
- [9] J.-T. Wei *et al.* (Belle Collaboration), *Phys. Rev. Lett.* **103**, 171801 (2009).
- [10] B. Aubert, *et al.* (BABAR Collaboration), *Phys. Rev.* **D79**, 031102(R) (2009).
- [11] T. Aaltonen *et al.* (CDF Collaboration), *Phys. Rev. Lett.* **108**, 081807 (2012).
- [12] R. Aaij *et al.* (LHCb Collaboration), arXiv:1512.04442.
- [13] S. Chatrchyan *et al.* (CMS Collaboration), *Phys. Lett.* **B727**, 77 (2013).
- [14] K.S.M.Lee, Z. Ligeti, I.W. Stewart, and Frank J. Tackmann, *Phys. Rev.* **D75**, 034016 (2007).

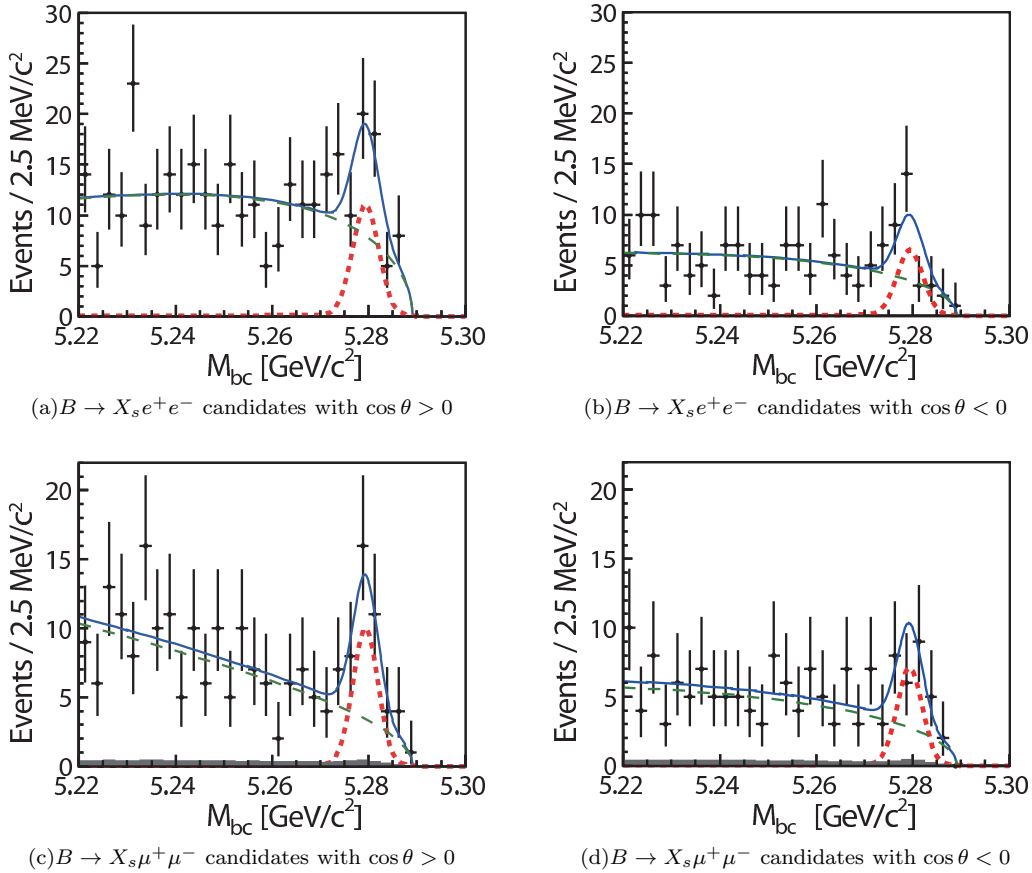


FIG. 2. M_{bc} distributions in 1st q^2 bin for (a) $B \rightarrow X_s e^+ e^-$ candidates with $\cos \theta > 0$, (b) $B \rightarrow X_s e^+ e^-$ candidates with $\cos \theta < 0$, (c) $B \rightarrow X_s \mu^+ \mu^-$ candidates with $\cos \theta > 0$, and (d) $B \rightarrow X_s \mu^+ \mu^-$ candidates with $\cos \theta < 0$. The thicker dashed curve (red) shows the sum of the signal and the self cross-feed components. The thinner dashed curve (green) shows the combinatorial background component. The filled histogram (gray) shows the peaking background component. The sums of all components are shown by the solid curve (blue).

- [15] M. Kobayashi and T. Maskawa, *Prog. Theor. Phys.* **49**, 652 (1973); N. Cabibbo, *Phys. Rev. Lett.* **10**, 531 (1963).
- [16] A. Abashian *et al.* (Belle Collaboration), *Nucl. Instrum. Meth. A* **479**, 117 (2002); also see the detector section in J. Brodzicka *et al.*, *Prog. Theor. Exp. Phys.* (2012) 04D001.
- [17] S. Kurokawa and E. Kikutani, *Nucl. Instrum. Meth. A* **499**, 1 (2003), and other papers included in this volume; T. Abe *et al.*, *Prog. Theor. Exp. Phys.* (2013) 03A001 and following articles up to 03A011.
- [18] A. Ali, P. Ball, L.T. Handoko, and G. Hiller, *Phys. Rev.* **D61**, 074024 (2000).
- [19] F. Kruger and L.M. Sehgal, *Phys. Lett.* **B380**, 199 (1996).
- [20] A. Ali and E. Pietarinen, *Nucl. Phys.* **B154**, 519 (1979).
- [21] Y. Amhis *et al.*, arXiv:1207.1158 and online update at <http://www.slac.stanford.edu/xorg/hfag/>
- [22] E. Nakano, *Nucl. Instrum. Meth. A* **494**, 402 (2002).
- [23] M. Feindt and U. Kerzel, *Nucl. Instrum. Meth. A* **559**, 190 (2006).
- [24] We define the total visible energy $E_{\text{vis}} = \sum_i E_i^*$, and the missing mass $M_{\text{miss}} = \sqrt{(2E_{\text{beam}}^* - \sum_i E_i^*)^2 - \sum_i |\vec{p}_i^*|^2}$, where (\vec{p}_i^*, E_i^*) are the reconstructed four-momenta in the $\Upsilon(4S)$ rest frame of all tracks assumed to be pions and all photons in the event.
- [25] The Fox-Wolfram moments were introduced in G.C. Fox and S. Wolfram, *Phys. Rev. Lett.* **41**, 1581 (1978); The modified moments used in this Letter are described in S.H. Lee *et al.* (Belle Collaboration), *Phys. Rev. Lett.* **91**, 261801 (2003).
- [26] H. Albrecht *et al.* (ARGUS Collaboration), *Phys. Lett. B* **241**, 278 (1990).
- [27] P. Ball and R. Zwicky, *Phys. Rev.* **D71**, 014015 (2005).
- [28] P. Ball and R. Zwicky, *Phys. Rev.* **D71**, 014029 (2005).
- [29] C. Schwanda *et al.* (Belle Collaboration), *Phys. Rev.* **D75**, 032005 (2007).
- [30] A. Limosani *et al.* (Belle Collaboration), *Phys. Rev. Lett.* **103**, 241801 (2009).
- [31] R. Aaij *et al.* (LHCb Collaboration), *Phys. Rev.* **D88**, 052002 (2013).

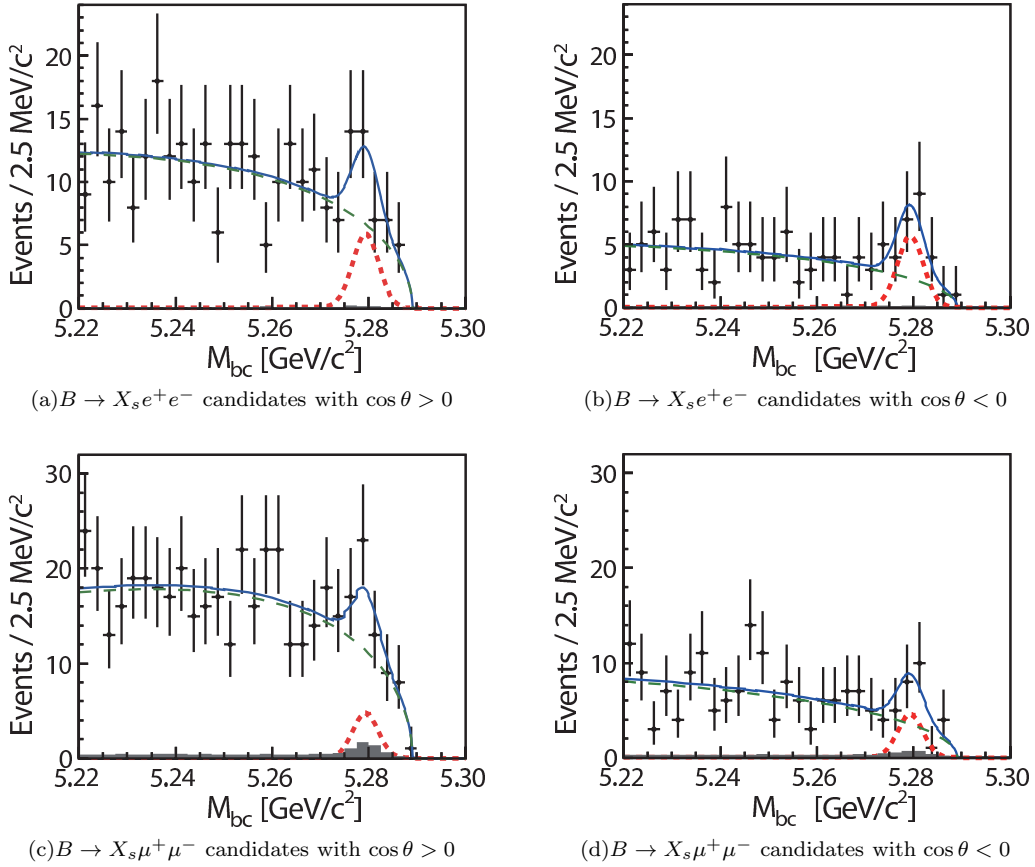


FIG. 3. M_{bc} distributions in 2nd q^2 bin for (a) $B \rightarrow X_s e^+ e^-$ candidates with $\cos \theta > 0$, (b) $B \rightarrow X_s e^+ e^-$ candidates with $\cos \theta < 0$, (c) $B \rightarrow X_s \mu^+ \mu^-$ candidates with $\cos \theta > 0$, and (d) $B \rightarrow X_s \mu^+ \mu^-$ candidates with $\cos \theta < 0$. The thicker dashed curve (red) shows the sum of the signal and the self cross-feed components. The thinner dashed curve (green) shows the combinatorial background component. The filled histogram (gray) shows the peaking background component. The sums of all components are shown by the solid curve (blue).

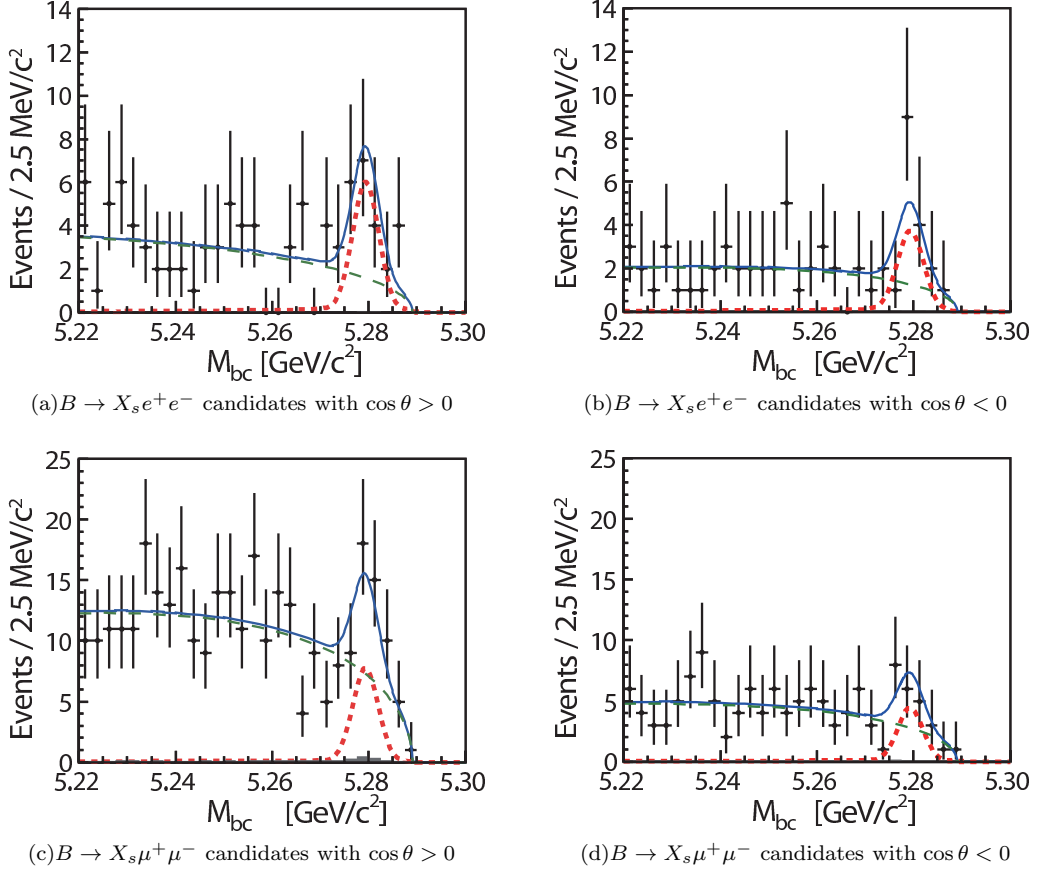


FIG. 4. M_{bc} distributions in 3rd q^2 bin for (a) $B \rightarrow X_s e^+ e^-$ candidates with $\cos \theta > 0$, (b) $B \rightarrow X_s e^+ e^-$ candidates with $\cos \theta < 0$, (c) $B \rightarrow X_s \mu^+ \mu^-$ candidates with $\cos \theta > 0$, and (d) $B \rightarrow X_s \mu^+ \mu^-$ candidates with $\cos \theta < 0$. The thicker dashed curve (red) shows the sum of the signal and the self cross-feed components. The thinner dashed curve (green) shows the combinatorial background component. The filled histogram (gray) shows the peaking background component. The sums of all components are shown by the solid curve (blue).

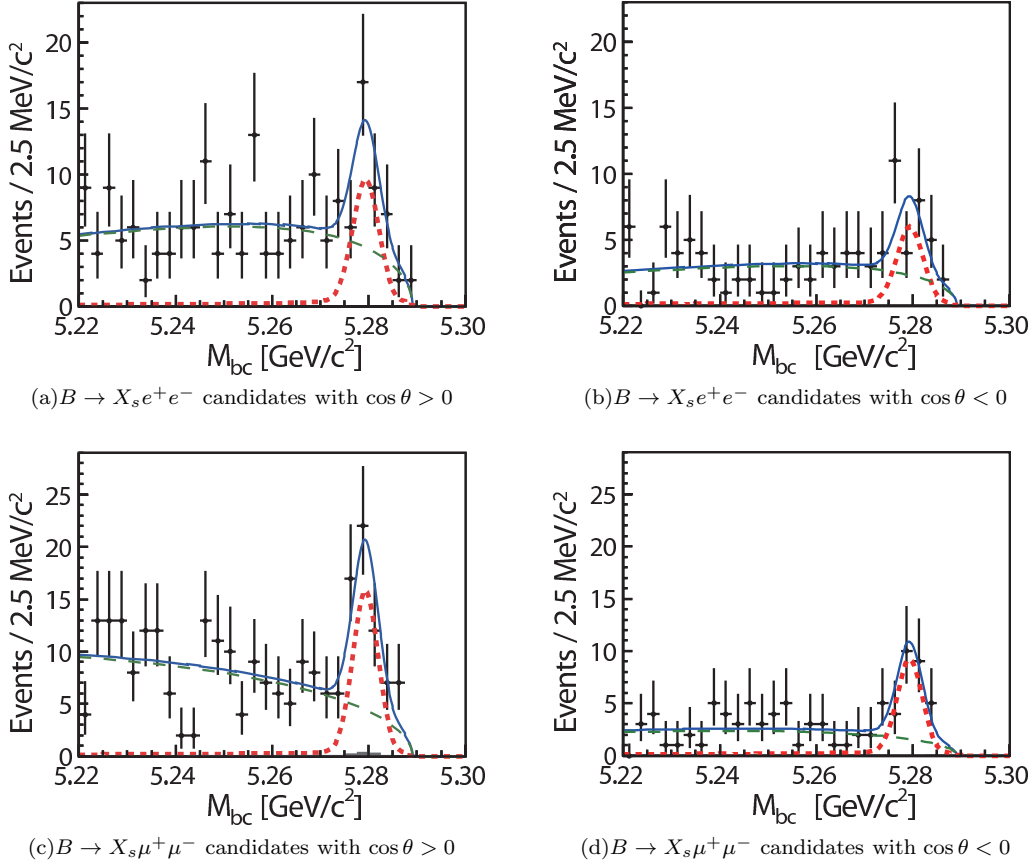


FIG. 5. M_{bc} distributions in 4th q^2 bin for (a) $B \rightarrow X_s e^+ e^-$ candidates with $\cos\theta > 0$, (b) $B \rightarrow X_s e^+ e^-$ candidates with $\cos\theta < 0$, (c) $B \rightarrow X_s \mu^+ \mu^-$ candidates with $\cos\theta > 0$, and (d) $B \rightarrow X_s \mu^+ \mu^-$ candidates with $\cos\theta < 0$. The thicker dashed curve (red) shows the sum of the signal and the self cross-feed components. The thinner dashed curve (green) shows the combinatorial background component. The filled histogram (gray) shows the peaking background component. The sums of all components are shown by the solid curve (blue).

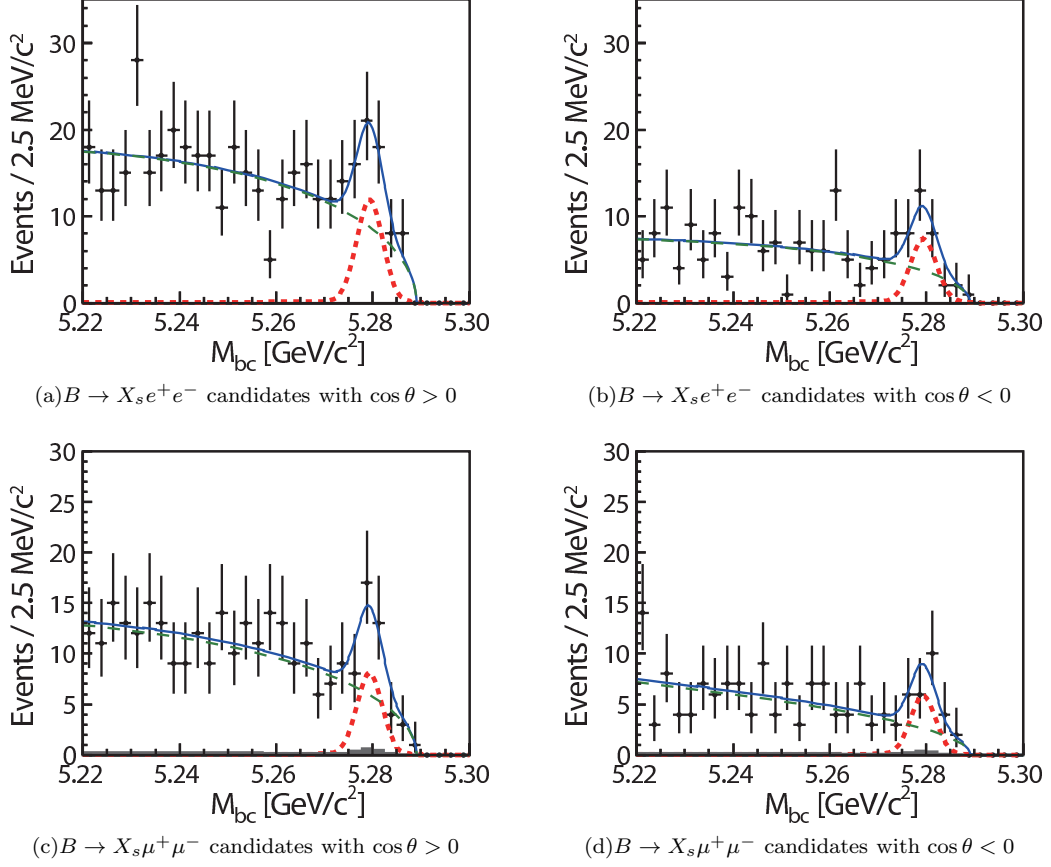


FIG. 6. M_{bc} distributions in the low- q^2 region, $1 < q^2 < 6 \text{ GeV}^2$ for (a) $B \rightarrow X_s e^+ e^-$ candidates with $\cos \theta > 0$, (b) $B \rightarrow X_s e^+ e^-$ candidates with $\cos \theta < 0$, (c) $B \rightarrow X_s \mu^+ \mu^-$ candidates with $\cos \theta > 0$, and (d) $B \rightarrow X_s \mu^+ \mu^-$ candidates with $\cos \theta < 0$. The thicker dashed curve (red) shows the sum of the signal and the self cross-feed components. The thinner dashed curve (green) shows the combinatorial background component. The filled histogram (gray) shows the peaking background component. The sums of all components are shown by the solid curve (blue).

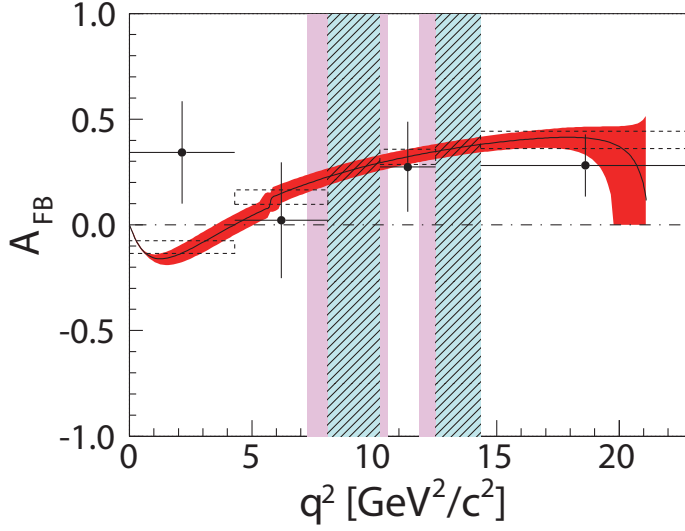


FIG. 7. Measured \mathcal{A}_{FB} as a function of q^2 . The curve (black) with the band (red) and dashed boxes (black) represent the SM prediction while filled circles with error bars show the fit results. The J/ψ and $\psi(2S)$ veto regions are shown as teal hatched regions. For the electron channel, the pink shaded regions are added to the veto regions due to the large bremsstrahlung effect. The uncertainty on the SM prediction is estimated by varying the b -quark mass ($4.80 \pm 0.15 \text{ GeV}/c^2$), the s -quark mass ($0.20 \pm 0.10 \text{ GeV}/c^2$), and the renormalization scale ($\mu = 2.5$ and 5 GeV) [4, 7]. The lower edge of the uncertainty is set to zero in the q^2 region larger than maximum possible value, which is determined by the masses of the bottom and strange quarks.